Appl. Phys. A 86, 283–288 (2007)
DOI: 10.1007/s00339-006-3760-4

Applied Physics A
Materials Science & Processing

L.E.F. FOA TORRES[1,2]
S. ROCHE[2,✉]

Electron–phonon induced conductance gaps in carbon nanotubes

[1] CEA/LETI, 17 rue des Martyrs, 38054 Grenoble, France
[2] CEA/DSM/DRFMC/SPSMS/GT, 17 avenue des Martyrs, 38054 Grenoble, France

Received: 15 September 2006/Accepted: 12 October 2006
Published online: 21 November 2006 • © Springer-Verlag 2006

ABSTRACT This work presents a theoretical study of quantum charge transport through zigzag and armchair carbon nanotubes in the presence of electron–phonon interaction. By using a non-perturbative description of the electron–phonon coupling in Fock space, one reveals the occurrence of a transmission gap opening at half the optical $A_1(L)$ phonon energy, $\hbar\omega_0/2$, above (below) the charge neutrality point associated with phonon emission (absorption). This mechanism, which is prevented at low bias voltages by Pauli blocking, develops when the system is driven out of equilibrium (high bias voltages). This yields an onset of current saturation of about 30 μA, which brings a completely novel perspective to understand electrical characteristics of nanotube-based devices.

PACS 73.63.Fg; 72.10.Di; 73.23.-b; 05.60.Gg

1 Introduction

The geometrical arrangement of carbon atoms to form nanostructures or low-dimensional systems is at the origin of unprecedented novel physical phenomena and properties. Indeed, they opened new directions for science and technology. The discoveries of buckminsterfullerene (C_{60}) [1] and carbon nanotubes (CNTs) [2] have benefited from the emerging quantum effects in low-disorder nano-objects. These carbon-based nano-object systems show some further similarities with the whole class of π-conjugated systems [3], in which σ-bonding is ensured by three out of the four valence electrons of carbon, whereas the remaining one participates in π-bonding, with a delocalized electronic population extended over long length scales. Notwithstanding, pure (undoped) π-conjugated systems efficiently lower their total energy by bond dimerization (alternating short and long bonds), bringing the system to a semiconducting state (with a typical gap in the order of 1.5 eV). This mechanism, referred to as the Peierls transition, prevents the synthesis of all carbon-based metallic systems of high crystalline order, and with large charge mobilities.

In contrast, CNTs offer the possibility for engineering quasi-one-dimensional ballistic conductors, owing to their anomalously low sensitivity to disorder-induced backscattering [4] and unique spectral features [5]. In these nanomaterials, the Peierls instability is inefficient to open a significant energy gap [6–11], and the existence of semiconducting nanotubes results from well-defined helical symmetry dependent selection rules, that forbid the existence of eigenstates at the Fermi level. The associated energy gap is diameter dependent and of pure topological origin [12].

Low-energy electronic properties of carbon nanotubes have been intensively studied over recent years. Depending on their coupling strength with contact electrodes, small-diameter metallic nanotubes are found to either display unprecedented ballistic transport over micron scales [13, 14] or exhibit signatures of non-Fermi-liquid behavior [15]. In large-diameter multiwall nanotubes or intentionally doped CNTs, the enhanced contribution of intrinsic disorder drives the system from weakly [16, 17] to strongly localized regimes [18], as long as the electronic phase coherence remains conserved. Fascinating magneto-transport properties result from the entangled contribution of field-dependent band structures and quantum interference effects [19].

Differently, high-energy properties are much less understood and strongly debated. Indeed, even if ballistic transport dominates in the low-bias regime, by increasing the potential bias across the nanotubes, the contribution of electron–phonon mediated backscattering is steadily enhanced, up to a saturation regime where intrinsic dissipation becomes dominant over current drift [13, 14, 20, 21]. This brings serious performance limitations of CNT-based field-effect transistors [22], but also raises fundamental questions about the nature of inelastic quantum transport in these unique objects [23–29].

In the high-bias regime, several attempts to relate the measured quantum conductance to some inelastic scattering lengths have been reported [30]. These estimations of inelastic scattering lengths assume the full applicability of the Fermi golden rule (FGR), that is, the validity of the perturbative regime for treating electron–phonon coupling and decoupling of the vibrational and electronic degrees of freedom. However, electron–phonon coupling yields important modifications of both electronic and phonon band structures. In the phonon dispersion of the material, one finds a singular behavior for certain $\boldsymbol{q}$ vectors and phonon branches, which is referred to as the Kohn anomaly [31] and which is driven by e–ph coupling. Similarly, the activation of vi-

✉ Fax: +33-(0)4-3878-3381,
E-mails: stephan.roche@cea.fr, luisfoa@gmail.com

brational modes has also some direct influence on the electronic spectra of CNTs. This has been initially evidenced through ab initio calculations, showing how the electronic band structure is modified in time, owing to time-dependent phonon-induced bond alternation [32]. For longitudinal optical modes, the π–π electronic band structure for metallic CNTs shows a time-dependent gap oscillation [32], which severely limits a rigorous application of the FGR and subsequent use of semiclassical-like transport methods. This time-dependent phenomenon has been shown to strongly degrade the coherent part of the Kubo quantum conductance [27].

In a previous paper [33], by implementing a quantum mechanical treatment of electron–phonon interaction in computing inelastic quantum transport, we have shown that the coupling of electrons with optical $A_1(L)$ phonons in $(N, 0)$ zigzag tubes is at the origin of an energy gap opening at $\hbar\omega_0/2$ above (below) the charge neutrality point (CNP), owing to phonon emission (absorption). This novel many-body mechanism, which is prevented at low bias by Pauli blocking, is activated when driving the system out of equilibrium (high-bias regime).

Here, this prior study is extended and generalized, and these phenomena are explored for the case of armchair CNTs. Besides, the theoretical description developed in [33] is deepened, and its connections with other schemes established. In Sect. 2, we focus on different possible Hamiltonian descriptions for the e–ph interaction and discuss the links between them. Specifically, a road map that links a full quantum description to a one-body time-dependent scheme and a mean-field approach is proposed. In Sect. 3, the full many-body scheme is outlined. In Sect. 4, this general scheme is applied to the case of optical modes in zigzag and armchair CNTs, while the conclusions are given in Sect. 5.

2 Hamiltonian description for the electron–phonon interaction: from a mean-field approach to a full quantum description

In this section, the effect of vibrations on the electronic transport is modeled. Our starting point is the elaboration of the Hamiltonian for the coupled e–ph system. For simplicity, an infinite CNT is considered and the electrons are allowed to interact with phonons only in the central part of the CNT. The Hamiltonian of the system can be written as a sum of an electronic part, a phonon part and an electron–phonon interaction term:

$$H = H_{\mathrm{e}} + H_{\mathrm{ph}} + H_{\mathrm{e-ph}} \,. \tag{1}$$

The electronic part is encoded through a π-orbital effective model (i.e. a single π-orbital per carbon atom):

$$H_{\mathrm{e}} = \sum_i E_i c_i^+ c_i - \gamma_0 \sum_{\langle i,j\rangle} \left[c_i^+ c_j + \mathrm{h.c.}\right] , \tag{2}$$

where c_i^+ and c_i are the creation and annihilation operators for electrons at site i and γ_0 is the π–π integral overlap; note that the second summation is restricted to nearest neighbors in the CNT. Let us consider a single phonon mode of energy $\hbar\omega_0$. Then, the phonon term is simply

$$H_{\mathrm{ph}} = \hbar\omega_0 b^+ b \,, \tag{3}$$

where b^+ and b are the phonon operators.

The last contribution describes the e–ph interaction term. Lattice vibrations will produce a time modulation of the bond's length thereby changing the hopping matrix elements. Our starting point to account for these phenomena is the Su–Schrieffer–Heeger Hamiltonian, where the contribution arising from the phonons is found by assuming a phonon modulation of the electronic coupling terms [34–36], keeping only the linear corrections to the atomic displacements from equilibrium. This reads

$$\gamma_{i,j} = \gamma_0 + \alpha\widehat{\delta}_{i,j} \cdot \delta Q_{i,j} \,, \tag{4}$$

where $\widehat{\delta}_{i,j}$ is a unit vector in the bond direction, whereas $\delta Q_{i,j}$ sets the relative displacement of the neighboring carbon atoms, and α is the e–ph coupling strength defined as the derivative of γ_0 with respect to the bond length displacement. At this point several descriptions are available. One possibility is to proceed by performing a further quantization of the atomic displacements. This gives the many-body e–ph interaction term

$$H_{\mathrm{e-ph}} = \sum_{\langle i,j\rangle_{\mathrm{vib}}} \left[\gamma_{i,j}^{\mathrm{e-ph}}\, c_i^+ c_j (b^+ + b) + \mathrm{h.c.}\right] , \tag{5}$$

where the e–ph interaction is allowed only in a finite section of length L of the CNT, b and b^+ are the phonon operators and the e–ph matrix elements $\gamma_{i,j}^{\mathrm{e-ph}}$ are generally given by

$$\gamma_{i,j}^{\mathrm{e-ph}} = \alpha\sqrt{\hbar/\left(2m\omega_0\right)}\widehat{\delta}_{i,j} \cdot \left(\widehat{e}_i - \widehat{e}_j\right) , \tag{6}$$

where $\widehat{e}_i$ is the phonon mode eigenvector which gives the atomic displacements from the equilibrium positions.

Note that in contrast to the Holstein model where the e–ph interaction is local, coupling to a non-local vibrational eigenmode is here described via a Su–Schreiffer–Heeger (SSH) Hamiltonian [34, 35]. This is crucial to obtain a realistic description of the e–ph interaction.

In general, it is not easy to solve the interacting e–ph problem quantum mechanically. An alternative is to encode the effect of e–ph interaction through a time-dependent modulation of the hopping matrix elements, i.e.

$$\gamma_{i,j} = \gamma_0 + \gamma_1 \cos(\omega_0 t + \varphi_{i,j}) \,. \tag{7}$$

This leads to a one-body time-dependent Hamiltonian [27, 37]

$$H(t) = \sum_i E_i c_i^+ c_i - \sum_{\langle i,j\rangle} \gamma_{i,j}(t) \left[c_i^+ c_j + \mathrm{h.c.}\right] .$$

Note that, in this case, ω_0 acquires the meaning of a frequency whereas in (5) $\hbar\omega_0$ is relevant as a true energy. This approximation can be seen as a replacement of the phonon field operators in (5) by a time-dependent function of time with well-defined amplitude and phase.

From this time-dependent picture we can see that in the $\omega_0 \to 0$ limit the atomic positions are frozen. This allows the use of a mean-field description where the configuration coordinates are constrained to those that minimize the total

energy of the system (electronic plus elastic). Note that the new equilibrium positions can differ from the ones in the absence of the electron–phonon interaction, leading to a static distortion of the lattice. This Born–Oppenheimer approximation allows for example the description of the dimerization in polyacetylene [34, 35].

For finite $\hbar\omega_0$, however, the Born–Oppenheimer or adiabatic approximation is not justified (the nuclei cannot be regarded as 'clamped'). Thus, it is necessary to go beyond this mean-field description either via the previously mentioned time-dependent (or semiclassical) Hamiltonian or by using a full quantum description as in (5). At this point the reader may wonder about the differences between these two alternative descriptions, semiclassical and quantum. We defer a hint on this question to Sect. 3.

3 Outline of the theoretical description

In order to investigate inelastic quantum transport for the e–ph Hamiltonian (5), the framework introduced in [38, 39] is followed. This scheme starts with rewriting the Hamiltonian in an appropriate basis for the e–ph Fock space (a single electron plus phonons), to construct an equivalent multichannel one-body problem. As a matter of illustration, let us consider an electron that tunnels from a left electrode (L) to a right electrode (R), while it interacts with a single phonon mode. Then, the asymptotic states in the non-interacting electrodes can be labeled by means of two indices: (X, n), where $X = \mathrm{L}, \mathrm{R}$ is the index corresponding to the electrode and n the number of phonon excitations in the system. This picture is equivalent to a multichannel one-body problem where the asymptotic states in the e–ph Fock space include both the electronic and new vibronic degrees of freedom. Each phonon mode adds a dimension to the problem.

Using this picture, the transmission $T_{(X,n)\to(Y,m)}$ and reflection $R_{(X,n)\to(Y,m)}$ probabilities between the different channels are computed by using standard Green's function techniques [40]. Once these probabilities are calculated, they are used as inputs to compute the non-equilibrium electron distributions in the leads (at finite temperature and bias voltage). This is done by using the self-consistent procedure developed in [43]. The electronic current can be obtained from these self-consistent distributions, which take into account the Pauli exclusion principle for the different competing elastic and inelastic processes.

It must be emphasized that in this approach the e–ph interaction is not assumed to produce phase randomization since the quantum phases are fully conserved in this coherent description. Instead of calculating transition rates, the complex quantum amplitude for each state in the Fock space is obtained. Another interesting point to notice is that the solution of the interacting Hamiltonian is obtained by truncating the Fock space including only the states within some range of n. This range can be enlarged until the solution converges, allowing for a variational, non-perturbative, calculation. For the interested reader, this approach has been applied to a variety of problems including vibration-assisted tunneling in Scanning Tunneling Microscopy experiments [41], transport through molecules [42, 43] and resonant tunneling in double-barrier heterostructures [40].

3.1 *Connection with the time-dependent picture*

As noted in [44], the connection between this scheme and the semiclassical description mentioned in Sect. 2 can be established by using Floquet theory [45–47] to solve the time-dependent problem associated with the model given by (7). By rewriting the time-dependent problem in Floquet space, it can be reduced to a higher-dimensional time-independent problem. Floquet or Sambe space is just the composed Hilbert space $R \otimes T$, where R is the space of functions in real space and T is the space of periodic functions with period $\tau = 2\pi/\omega_0$. The space T is spanned by the set of orthonormal Fourier vectors $\langle t|m\rangle \equiv \exp(im\omega_0 t)$, where m is an integer. Then, given a basis of Hilbert space $\{|\varphi_i\rangle\}$, a suitable basis in Floquet space is given by $\{|\varphi_i, m\rangle = |\varphi_i\rangle \otimes |m\rangle\}$. The resemblance with the mapping technique for the quantum e–ph problem described before is clear. In formal terms it can be expressed as an isomorphism between the states in Fock space and those in Floquet space [45]. Some key differences [44, 48] are: (a) that for the case of phonons the temperature enters naturally in the population of the different channels. This is not the case for a time-dependent potential. (b) In contrast to the situation for the time-dependent potential, where the index m plays the role of the number of phonons in the system, the number of phonons in the system is bounded from below, $n \geq 0$. (c) Another important difference is that the presence of the matrix elements for phonon emission and absorption depends on the number n of phonons present in the system. In contrast, the matrix elements in Floquet space between states of different m are independent of it.

3.2 *Determination of the e–ph Hamiltonian matrix elements*

In Sect. 4, the focus is made on transport through zigzag and armchair CNTs in the presence of e–ph interaction with an $A_1(L)$ phonon mode (at the Γ point of the Brillouin zone). One first describes explicitly the matrix elements of the e–ph Hamiltonian (5). These terms are essentially provided by the projection of the bond direction on the relative displacement of the atoms from their equilibrium positions, $\widehat{\delta}_{i,j} \cdot (\widehat{d}_i - \widehat{d}_j)$. The atomic displacements for the case corresponding to the $A_1(L)$ mode in zigzag and armchair CNTs are represented in Fig. 1. For zigzag tubes, it can be shown that $\gamma_{i,j}^{\mathrm{e-ph}} = \gamma_0 = 2\alpha\sqrt{\hbar/(2m\omega_0)}$, with (i, j) corresponding to a bond that is parallel to the axis direction, whereas $\gamma_{i,j}^{\mathrm{e-ph}} = -\gamma_0 \cos(\pi/3)$ describes the coupling for bonds that are tilted with respect to the CNT axis. The e–ph matrix elements for the case of armchair CNTs can be obtained in a similar way.

4 Results and discussion: phonon-induced energy gaps, manifestations in quantum transport

In this section, numerical results for transport through zigzag and armchair CNTs in the presence of e–ph interaction with an $A_1(L)$ phonon mode are shown and discussed. All the energies are expressed in units of the C–C hopping matrix element γ_0 (~ 2.77 eV). The phonon energy is taken as $\hbar\omega_0 \simeq 0.07\gamma_0$ [32], while the parameter $\alpha \simeq \alpha_0 = 7$ eV/Å is estimated from [51, 52].

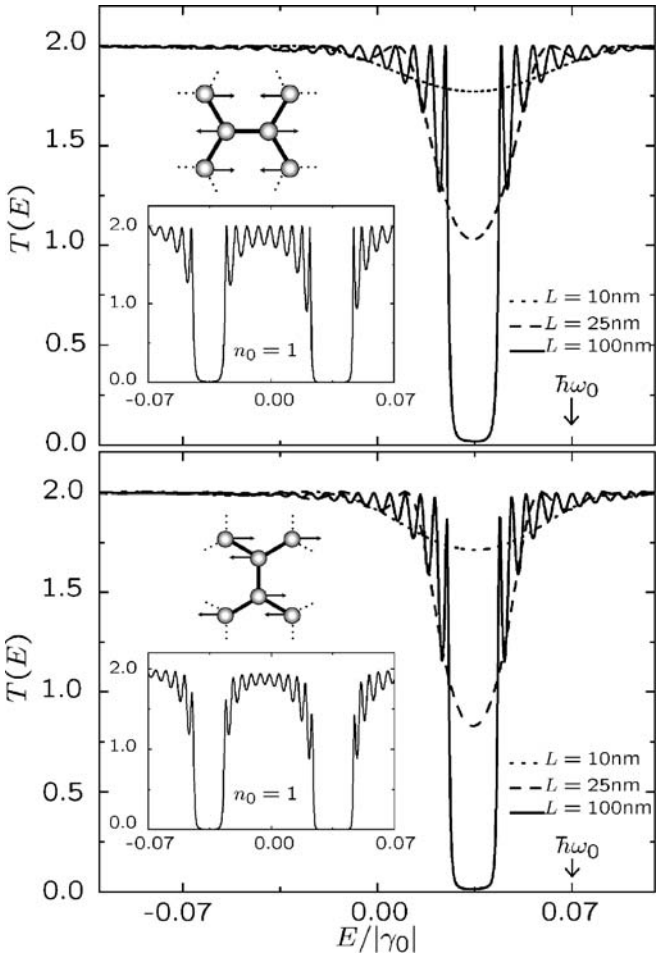

FIGURE 1 Total transmission probability as a function of the energy of the incident electrons for $n_0 = 0$. The *top figure* corresponds to zigzag (24, 0) CNTs while the *bottom figure* corresponds to armchair (10, 10) CNTs. In the *insets* we show the same information for $n_0 = 1$. The results correspond to CNTs in the presence of e–ph interaction with an $A_1(L)$ mode inducing displacements along the axis direction as schematically represented in each figure

In Fig. 1 (top panel), the total transmission probability $T(E) = \sum_n T_{(L,n_0)\to(R,n)}(E)$ is shown as a function of the incident electron kinetic energy E for a zigzag tube if no phonons are present in the system before the occurrence of the scattering process ($n_0 = 0$). The main feature is the onset of a dip centered at $\hbar\omega_0/2$ above the CNP which progressively deepens as the tube length increases, until a full gap opens for $L \simeq 100$ nm. The inelastic component of the total transmission shown in the plot is orders of magnitude smaller than the elastic contribution in all the shown energy range. However, one observes that the reduction of the transmission in the dip region is due to a complementary increase in the inelastic reflection by phonon emission. Similar results are found for armchair CNTs; see Fig. 1 (bottom panel).

The total transmission probability when one phonon is already available for scattering ($n_0 = 1$) is shown in Fig. 1 for zigzag tubes (top panel, inset) and armchair tubes (bottom panel, inset). There are two main differences with the case $n_0 = 0$: the width of the gap at $E \sim \hbar\omega_0/2$ is approximately $\sqrt{2}$ larger than in the prior case owing to stimulated phonon emission. The second important difference is the appearance of a second gap at $E \sim -\hbar\omega_0/2$. The analysis of the different elastic and inelastic components of the transmission and reflection probabilities reveals that this decrease in the transmission is complemented by an increase in the inelastic backscattering by phonon absorption.

To explain these results, let us consider an infinite tube in the presence of e–ph interaction. For simplicity we will consider the case of zigzag $(N, 0)$ tubes, where the use of a mode space approach [49, 50] simplifies the analysis. The idea is to rewrite the problem in the basis that diagonalizes H_e for each layer of carbon atoms perpendicular to the tube axis. Thus, the Hilbert space can be expanded in terms of the states $|l_q\rangle$ corresponding to the different circumferential modes q ($q = 0, 1, \ldots, N-1$) localized at the lth layer of the tube. In the absence of static disorder, the electronic Hamiltonian H_e does not couple the different modes, and the different subbands correspond to linear chains with alternating hoppings γ_0 and $\gamma_q = 2\gamma_0 \cos(q\pi/N)$ with dispersion relations $\varepsilon^{(0)}(k) = \pm\sqrt{\gamma_0^2 + \gamma_q^2 + 2\gamma_0\gamma_q \cos(3ka_{cc}/2)}$. Furthermore, since the symmetry of the considered phonon mode prevents the coupling between different circumferential modes, one obtains N independent problems for each value of q. When N is an integer multiple of three, the tube is metallic and the subbands contributing to the density of states close to the CNP correspond to $q = N/3, 2N/3$.

The Fock space for the coupled e–ph system can be expanded either in terms of the basis states $\{|l_q, n\rangle = |l_q\rangle \otimes |n\rangle\}$, where $|n\rangle$ corresponds to the state with n phonons in the system, or, alternatively, $\{|k, n\rangle = |k\rangle \otimes |n\rangle\}$, where $|k\rangle$ is a plane wave in mode space with wave vector k along the axis direction. The interacting Hamiltonian in the Fock space for a given q is represented in Fig. 2 (top panel). In the following, we consider the mode with $q = N/3$, although a similar argument holds for $q = 2N/3$. The electronic part of the Hamiltonian for $q = N/3$ is an ordered chain with nearest-neighbor matrix elements γ_0 ($\gamma_q = \gamma_0$ for $q = 2N/3$). In contrast, the e–ph hopping matrix elements $\left(\gamma_{i,j}^{\text{e-ph}}\right)_{q=N/3}$ are not homogeneous from one layer to the next but have alternating values $\gamma_0^{\text{e-ph}}$ and $-\gamma_0^{\text{e-ph}} \cos(\pi/3)$, thereby doubling the layer periodicity of the many-body Hamiltonian.

In the absence of e–ph coupling, one obtains disconnected chains associated with the different values of n, each with unperturbed dispersion relation $\varepsilon_n^{(0)} = \varepsilon_n^{(0)}(k)$ (see Fig. 2). Of particular interest are the states $|k_+ = \pi/2a + |\delta k|, 0\rangle$ and $|k_+ - K, 1\rangle$ (black circles), where $a = 3a_{cc}/4$ and $K = 2\pi/(2a)$ is the wave vector associated with the lattice period by of the overall Hamiltonian H. For vanishing e–ph coupling, these states have the same total energy $\varepsilon_0^{(0)}(k_+) = \varepsilon_1^{(0)}(k_+ - K) = \hbar\omega_0/2$. When the e–ph interaction is switched on, these Fock states are mixed owing to the spatial periodicity introduced by $H_{\text{e-ph}}$, i.e. $\langle k_+ - K, 1| H_{\text{e-ph}} |k_+, 0\rangle = \Delta\gamma^{\text{e-ph}} \equiv (3/2)\,\gamma_0^{\text{e-ph}} \neq 0$ [53]. The degeneracy is thus lifted, giving rise to the opening of an energy gap in $\varepsilon_0(k)$ and $\varepsilon_1(k)$ of width $2\left|\Delta\gamma^{\text{e-ph}}\right|$ around $\varepsilon = \hbar\omega_0/2$ (inset in Fig. 2).

Therefore, an incoming electron with a wave vector k in the Fock state $|k, n\rangle$ will contain, as k approaches k_+ (or $-k_+ + K$), an increasing admixture of $|k - K, n+1\rangle$ (or $|k + K, n-1\rangle$) leading to a Bragg type of inelastic scattering.

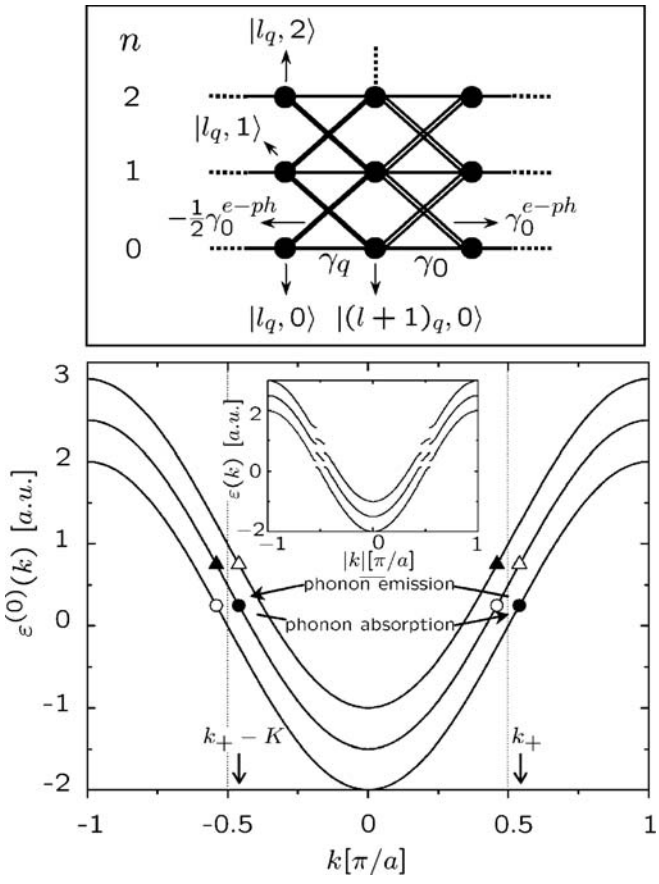

FIGURE 2 *Top*: representation of the many-body Hamiltonian in Fock space for a circumferential mode q (note the two-layer periodicity) in zigzag CNTs. *Solid circles* represent states in Fock space while the *lines* are off-diagonal couplings. *Bottom*: scheme for the unperturbed ($H_{e-ph} = 0$) dispersion relations corresponding to $n = 0, 1, 2$ for the mode $q = N/3$. The states marked with identical symbols correspond to degenerate states of the coupled e–ph system. These degeneracies are lifted by the e–ph interaction leading to the opening of energy gaps at $\hbar\omega_0/2$ above (below) the band center as represented in the *inset*

The origin of this mechanism is the modification of the translational symmetry of the system driven by the e–ph interaction which involves no static distortion of the lattice. Since the total energy ε also contains the vibronic energy, we note that in the previous argument the gap in $\varepsilon_0(k)$ manifests as a transmission gap for kinetic electronic energies $E \sim \hbar\omega_0/2$ while the gap in $\varepsilon_1(k)$ leads to a transmission gap at $E \sim -\hbar\omega_0/2$. A similar effect holds for the other states marked as symbols of the same kind in Fig. 2. For the subband with $q = 2N/3$ the only difference is a sign in $\gamma_q = -\gamma_0$, which can be absorbed in the wavefunction by changing only the character of the low-energy states from bonding to anti-bonding. This results in the transmission gaps shown in Fig. 1, which are in quantitative agreement with the prior analysis.

Another interesting point to investigate is the scaling of the transmission minimum at the gap center, $T(E = \hbar\omega_0/2)$, as a function of the CNT length L (the length of the interacting region). This is shown in Fig. 3 for different values of α, the e–ph coupling strength. Solid lines correspond to zigzag tubes and dotted lines correspond to armchair tubes. Tunneling through the gap leads to a range of lengths where the transmission decays exponentially with L, i.e. $T \propto \exp(-L/\xi)$.

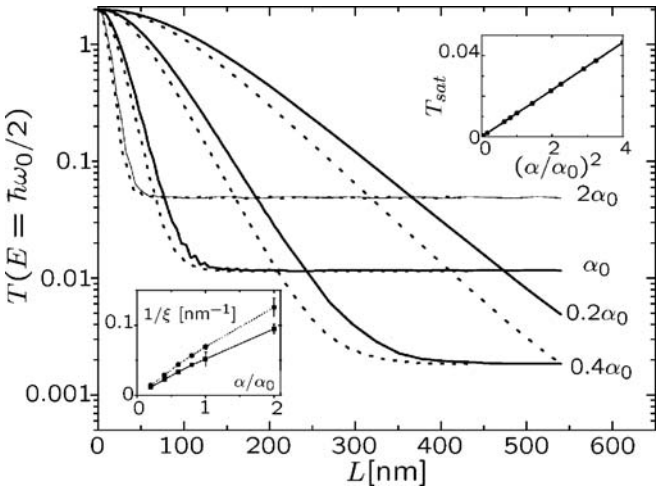

FIGURE 3 Total transmission probability at $E = \hbar\omega_0/2$ as a function of the tube length for $n = 0$; the other parameters are the same as in Fig. 1. *Solid lines* correspond to zigzag CNTs and *dotted lines* to armchair CNTs. The saturation value of the total transmission as a function of α^2 is shown in the *upper inset*. The *lower inset* shows the fitted inverse decay rates ($1/\xi$) as a function of α/α_0

The decay length ξ is inversely proportional to the energy gap $\Delta\gamma^{e-ph}$. The different geometries of zigzag and armchair tubes lead to different values of $\gamma_{i,j}^{e-ph}$, which cause different slopes of the exponential decay (see lower inset). Another interesting feature is the observed saturation for longer tubes. The saturation value T_{sat} as a function of α^2 (upper inset of Fig. 3) is associated with the small inelastic component of the transmission (phonon-assisted tunneling through the gap).

In the following the consequences of the prior study on the current–voltage characteristics of CNTs are explored. A first important observation is that due to the finite energy of the phonons, Pauli blocking will prevent the opening of the transmission gap at low bias voltage. In order to activate this mechanism, the system has to be driven out of equilibrium by applying a sufficiently high bias in between the voltage probes. To unveil the possible signatures of the proposed mechanism in the current–voltage characteristics, the effect of the bias

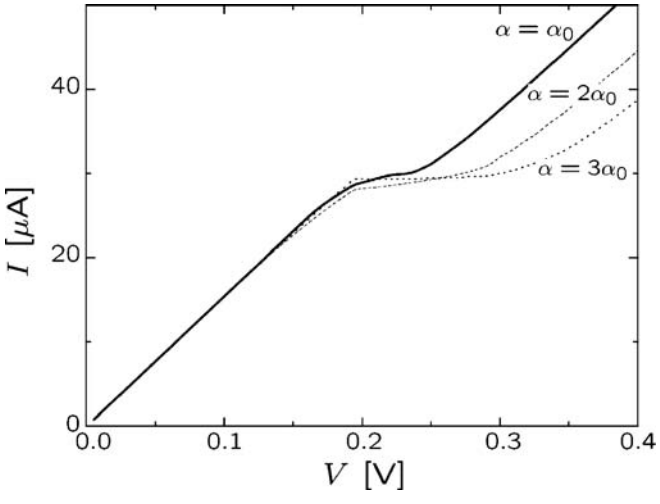

FIGURE 4 Current versus bias voltage for a 150-nm-long zigzag $(24, 0)$ tube. Different curves correspond to different values of α. *Solid lines* correspond to a fixed phonon population $n_0 = 0$

voltage is introduced into H_e by modifying the on-site energies of the π-orbitals, while the potential drop is assumed to be equally distributed at the two contacts. The current–voltage curves calculated from this model for different values of α and zero temperature are shown in Fig. 4. The main feature resulting from the gap opening is the onset of a current plateau observed at $V \sim \hbar\omega_0$ whose width scales linearly with α. Remarkably, one notes that the obtained saturation plateau, of approximately 30 μA, is in good agreement with experimental data [20]. This value exactly corresponds to $(4e/h)\hbar\omega_0$, while the linear slope at low bias is given by: $I/V = 4e^2/h$. As one continues to increase the bias voltage, the current starts to increase linearly. This is due to the lack of other ingredients in our model, such as electronic coupling with other phonon modes (such as those producing interband backscattering) or electrostatic effects.

5 Conclusions

In summary, we have studied inelastic quantum transport through CNTs in the presence of e–ph interaction with an $A_1(L)$ mode. By using a full quantum coherent approach, we showed that phonon emission (absorption) induces the opening of transmission gaps at $\hbar\omega_0/2$ above (below) the CNP. Due to the finite energy of the considered optical phonons, this effect is suppressed at low bias voltages and is activated for voltages in the order of $\hbar\omega_0$, generating the onset of a current plateau at ~ 30 μA for perfect contacts. For the case of semiconducting CNTs (not shown in this paper) with an intrinsic gap smaller than the phonon energy, we found that the predicted phonon induced gap remains.

While we have studied only the case of zigzag and armchair tubes, we expect similar effects for chiral tubes. Besides, the study of other phonon modes and the possible application to systems other than CNTs open new promising challenges.

REFERENCES

1 H. Kroto, J.R. Heath, S.C. O'Brien, R.F. Curl, R.F. Smalley, Nature (London) **318**, 62 (1985)
2 S. Iijima, Nature **354**, 56 (1991)
3 A.J. Heeger, S. Kivelson, J.R. Schrieffer, W.P. Su, Rev. Mod. Phys. **60**, 781 (1988)
4 C.T. White, T.N. Todorov, Nature **393**, 240 (1998)
5 J.W. Mintmire, C.T. White, Nature **394**, 29 (1998)
6 J.W. Mintmire, B.I. Dunlap, C.T. White, Phys. Rev. Lett. **68**, 631 (1992)
7 R. Saito, M. Fujita, G. Dresselhaus, M.S. Dresselhaus, Phys. Rev. B **46**, 1804 (1992)
8 K. Harigaya, M. Fujita, Phys. Rev. B **47**, 16 563 (1993)
9 A. Sedeki, L.G. Caron, C. Bourbonnais, Phys. Rev. B **62**, 6975 (2000)
10 M.T. Figge, M. Mostovoy, J. Knoester, Phys. Rev. Lett. **86**, 4572 (2001)
11 D. Connétable, G.M. Rignanese, J.C. Charlier, X. Blase, Phys. Rev. Lett. **94**, 015 503 (2005)
12 R. Saito, G. Dresselhaus, M.S. Dresselhaus, *Physical Properties of Carbon Nanotubes* (Imperial College Press, London, 1998)
13 A. Javey, J. Guo, M. Paulsson, Q. Wang, D. Mann, M. Lundstrom, H. Dai, Phys. Rev. Lett. **92**, 106 804 (2004)
14 J.Y. Park, S. Rosenblatt, Y. Yaish, V. Sazonova, H. Ustunel, S. Braig, T.A. Arias, P. Brouwer, P.L. McEuen, Nano Lett. **4**, 517 (2004)
15 M. Bockrath, D.H. Cobden, A.G. Rinzler, R.E. Smalley, L. Balents, P.L. McEuen, Nature **397**, 598 (1999)
16 F. Triozon, S. Roche, A. Rubio, D. Mayou, Phys. Rev. B **69**, 121 410 (2004)
17 S. Latil, S. Roche, D. Mayou, J.C. Charlier, Phys. Rev. Lett. **92**, 256 805 (2004)
18 J.C. Gómez-Navarro, P.J. De Pablo, J. Gomez-Herrero, B. Biel, F.J. Garcia-Vidal, A. Rubio, F. Flores, Nature Mater. **4**, 534 (2005)
19 S. Latil, F. Triozon, S. Roche, Phys. Rev. Lett. **95**, 126 802 (2005)
20 Z. Yao, C.L. Kane, C. Dekker, Phys. Rev. Lett. **84**, 2941 (2000)
21 E. Pop, D. Mann, J. Cao, Q. Wang, K. Goodson, H. Dai, Phys. Rev. Lett. **95**, 155 505 (2005)
22 J. Appenzeller, J. Knoch, M. Radosavljević, Ph. Avouris, Phys. Rev. Lett. **92**, 226802 (2006)
23 V. Perebeinos, J. Tersoff, P. Avouris, Phys. Rev. Lett. **94**, 086 802 (2005)
24 G. Pennington, N. Goldsman, Phys. Rev. B **68**, 086 802 (2005)
25 M. Lazzeri, S. Piscanec, F. Mauri, A.C. Ferrari, J. Robertson, Phys. Rev. Lett. **95**, 236 802 (2005)
26 M. Georghe, R. Gutierrez, N. Ranjan, A. Pecchia, A. Di Carlo, G. Cuniberti, Europhys. Lett. **71**, 438 (2005)
27 S. Roche, J. Jiang, F. Triozon, R. Saito, Phys. Rev. Lett. **95**, 076 803 (2005)
28 M.A. Kuroda, A. Cangellaris, J.P. Leburton, Phys. Rev. Lett. **95**, 266 803 (2005)
29 M. Lazzeri, F. Mauri, Phys. Rev. B **73**, 165 419 (2006)
30 X. Zhou, J.Y. Park, S. Huang, J. Liu, P.L. McEuen, Phys. Rev. Lett. **95**, 146 805 (2005)
31 S. Piscanec, M. Lazzeri, F. Mauri, A.C. Ferrari, J. Robertson, Phys. Rev. Lett. **93**, 185 503 (2004)
32 O. Dubay, G. Kresse, H. Kuzmany, Phys. Rev. Lett. **88**, 235 506 (2002)
33 L.E.F. Foa Torres, S. Roche, Phys. Rev. Lett. **97**, 076 804 (2006)
34 W.P. Su, J.R. Schrieffer, A.J. Heeger, Phys. Rev. Lett. **42**, 1698 (1979)
35 W.P. Su, J.R. Schrieffer, A.J. Heeger, Phys. Rev. B **22**, 2099 (1980)
36 G.D. Mahan, Phys. Rev. B **68**, 125 409 (2003)
37 H. Watanabe, T. Kawarabayashi, Y. Ono, J. Phys. Soc. Japan **74**, 1240 (2005)
38 E.V. Anda, S.S. Makler, H.M. Pastawski, R.G. Barrera, Braz. J. Phys. **24**, 330 (1994)
39 J. Bonča, S.A. Trugman, Phys. Rev. Lett. **75**, 2566 (1995)
40 L.E.F. Foa Torres, H.M. Pastawski, S.S. Makler, Phys. Rev. B **64**, 193 304 (2001)
41 N. Mingo, K. Makoshi, Phys. Rev. Lett. **84**, 3694 (2000)
42 H. Ness, A.J. Fisher, Phys. Rev. Lett. **83**, 452 (1999)
43 E.G. Emberly, G. Kirczenow, Phys. Rev. B **61**, 5740 (2000)
44 L.E.F. Foa Torres, Phys. Rev. B **72**, 245 339 (2005)
45 J.H. Shirley, Phys. Rev. **138**, B979 (1965)
46 H. Sambe, Phys. Rev. A **7**, 2203 (1973)
47 S. Kohler, J. Lehmann, P. Hänggi, Phys. Rep. **406**, 379 (2005)
48 D.F. Martínez, J. Phys. A **36**, 9827 (2003)
49 N. Mingo, L. Yang, J. Han, M.P. Anantram, Phys. Stat. Solidi B **226**, 79 (2001)
50 A. Svizhenko, M.P. Anantram, Phys. Rev. B **72**, 085 430 (2005)
51 D. Porezag, T. Frauenheim, T. Köhler, G. Seifert, R. Kaschner, Phys. Rev. B **51**, 12 947 (1995)
52 J. Jiang, R. Saito, G. Samsonidze, S. Chou, A. Jorio, G. Dresselhaus, M. Dresselhaus, Phys. Rev. B **72**, 235 408 (2005)
53 From the point of view of momentum conservation, this process can be seen as an Umklapp process. Electrons and phonons not only interact among themselves (e–ph processes) but also with the periodic potential (lattice). Thus, momentum conservation is defined modulo a reciprocal lattice vector